

Coupling of Josephson current qubits using a connecting loop

Mun Dae Kim* and Jongbae Hong

School of Physics, Seoul National University, Seoul 151-742, Korea

We propose a coupling scheme for the three-Josephson junction qubits which uses a connecting loop, but not mutual inductance. Present scheme offers the advantages of a large and tunable level splitting in implementing the controlled-NOT (CNOT) operation. We calculate the switching probabilities of the coupled qubits in the CNOT operations and demonstrate that present CNOT gate can meet the criteria for the fault-tolerant quantum computing. We obtain the coupling strength as a function of the coupling energy of the Josephson junction and the length of the connecting loop which varies with selecting two qubits from the scalable design.

PACS numbers: 85.25.Dq, 03.67.Lx, 74.50.+r

I. INTRODUCTION

The persistent current qubit using superconducting loop with three Josephson junctions has been proposed as a promising candidate for quantum computer^{1,2,3,4} owing to the advantages of relatively long decoherence time and possible scalability. The current qubit has shown quantum superposition³ and, recently, coherent time evolution⁴ between two quantum states. Therefore, the feasibility of the current qubit as a practical quantum computer has increased recently. In order to realize a practical quantum computer, qubits must be coupled with scalability and any selected pair of qubits should perform a universal logic gate. One of universal logic gates is composed of the controlled-NOT (CNOT) operations and the single-qubit rotations.^{5,6}

In this study we suggest a coupling scheme for CNOT operation and scalable design using the three-junction current qubit as our unit qubit whose feasibility as a single qubit has already been tested.^{1,2,3,4} Here we propose a design for coupling two qubits using a connecting loop. Two qubits are connected by a superconducting loop with Josephson junctions which carries a persistent current by effective piercing flux. The effective flux comes from the phase differences across the Josephson junctions common to the qubit loop and the connecting loop. We calculate coupling strength between two qubits as a function of the coupling energy of Josephson junction in connecting loop and the length of connecting loop which varies with selecting qubits from the scalable circuit.

Recent experiments on two coupled charge qubits have demonstrated coherent oscillation⁷ and CNOT gate operation.⁸ For the coupled three-Josephson junction qubits⁹ and the coupled current-biased Josephson junction qubits¹⁰ spectroscopy measurements have been performed, but the CNOT operation has not yet been demonstrated. It seems that, for the coupled three-Josephson junction qubits, the coupling strength between qubits is too weak to implement CNOT operation. Here we aim to propose a coupling scheme which is expected to have strong advantages in CNOT operation, since the coupling strength can be large enough to suppress the unwanted oscillation of the control qubit. In order

to obtain quantitative results we calculate the switching probabilities of the coupled qubit system in CNOT operation. For an appropriate range of parameters, target qubit oscillates and shifts to another state while the unwanted oscillation of control qubit can be suppressed, which can be implemented within the fault-tolerant criteria of quantum computing.^{5,6} Moreover present coupling scheme offers the tunable coupling strength and the selective coupling from the scalable design, which is crucial for implementation of practical quantum computing but is not provided by the previous coupling schemes.^{7,8,9,10} We also show that the coupling strength does not diminish rapidly as length of the connecting loop increases.

II. HAMILTONIAN OF THE COUPLED QUBITS

A pair of coupled qubits is drawn in Fig. 1 (a). Two qubits are coupled through a connecting loop. Using this coupled qubits as a basic unit, a possible design to achieve a scalable computing is presented in Fig. 1 (b). We ex-

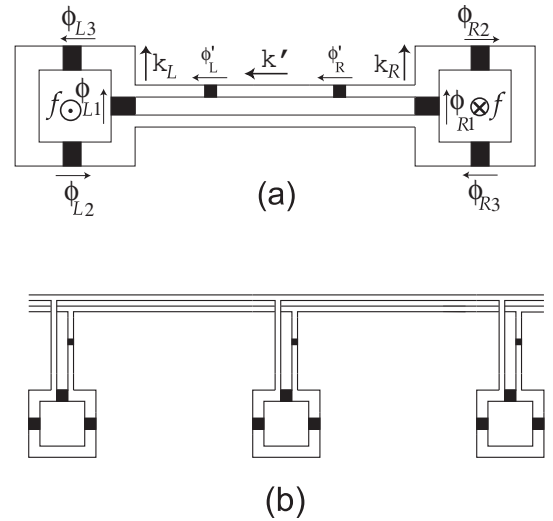


FIG. 1: (a) A pair of coupled qubits. (b) A part of the scalable quantum computing device. One unit is composed of a three-junction qubit, a dc-SQUID, and a connecting loop.

press the direction of the penetrating flux of the qubits oppositely in Fig. 1 (a), because two selected qubits are connected in a twisted way as shown in Fig. 1 (b). The two Josephson junctions in the connecting loop of Fig. 1 (a) denote the dc-SQUID's that enable tunable coupling and switching function for selective coupling. The wiring scheme connecting any pair of qubits is topologically the same. The interqubit magnetic crosstalk between the qubit islands can be neglected, since the induced flux of the three-Josephson junction loop is very weak and the qubit islands are separated far enough. In Fig. 1 (a) the weak magnetic interaction between the qubit loop and the connecting loop may exist even though the area of the connecting loop is very small. However, by manufacturing the connecting loop in such a way that the normal directions of the qubit loop and the connecting loop are perpendicular to each other, we can prevent this unwanted interaction.

The fluxoid quantization condition for a thin superconducting loop¹¹,

$$-\Phi_t + (m_c/q_c) \oint \vec{v}_c \cdot d\vec{l} = n\Phi_0 \quad (1)$$

with $q_c = 2e$, $m_c = 2m_e$, \vec{v}_c the average velocity of Cooper pairs, $\Phi_0 \equiv h/2e$ the superconducting unit flux quantum and Φ_t the total flux, can be represented as the periodic boundary condition for the wave function of the Cooper pairs including the phase evolution accumulated over the circumference of the loop with three Josephson junctions as follows,^{12,13}

$$k_n l = 2\pi n + 2\pi f_t - (\phi_1 + \phi_2 + \phi_3), \quad (2)$$

where k_n is the wave vector of the Cooper pairs, n an integer, l the circumference of the loop, and $f_t \equiv \Phi_t/\Phi_0$. Here ϕ_i is the phase difference across the i -th Josephson junction in a qubit.

Since the total flux is the sum of external and induced one, it is written as

$$f_t = f + \frac{L_s I}{\Phi_0} = f - \frac{\gamma l}{2\pi} k_n, \quad (3)$$

where $f \equiv \Phi_{\text{ext}}/\Phi_0$ and $\gamma \equiv L_s/L_K$. Here L_s is the self inductance and $L_K \equiv m_c l / A n_c q_c^2$ the kinetic inductance of the loop, where n_c is the density of Cooper pairs, A the cross section of the ring, and $m_c = 2m_e$ the mass of a Cooper pair. The dimensionless parameter γ can also be represented by the ratio of the energy scale such as $\gamma = E_K/E_L$ with $E_K \equiv \Phi_0^2/2L_K$ and $E_L \equiv \Phi_0^2/2L_s$. Here use of the current expression $I = -n_c A q_c \hbar k_n / m_c$ has been made. Then $k_n l$ of Eq. (2) is reexpressed as

$$(1 + \gamma)k_{R(L)}l = 2\pi n_{R(L)} + 2\pi f_{R(L)} - (\phi_{R(L)1} + \phi_{R(L)2} + \phi_{R(L)3}), \quad (4)$$

where $R(L)$ denotes the right (left) qubit and $k_{R(L)}$ is $k_n l$ of the right (left) qubit.

Since the value of γ for the three-Josephson junction qubit loop³ is very large such that $\gamma \approx 200$, Eq. (4) can be written as $\gamma k_{R(L)}l \approx 2\pi n_{R(L)} + 2\pi f_{R(L)} - (\phi_{R(L)1} + \phi_{R(L)2} + \phi_{R(L)3})$ and the boundary condition in Eq. (2) becomes

$$2\pi n + 2\pi f_t - (\phi_1 + \phi_2 + \phi_3) \approx 0. \quad (5)$$

Using the relation in Eq. (3) we can obtain the relation for the current in the qubit loop given by

$$I_{R(L)} = -\frac{\Phi_0}{L_s} \left(n_{R(L)} + f_{R(L)} - \frac{\phi_{R(L)1} + \phi_{R(L)2} + \phi_{R(L)3}}{2\pi} \right). \quad (6)$$

From this expression we can get for the effective potential $U_{\text{eff}}(\phi)$,

$$U_{\text{eff}}^{R(L)}(\phi_{R(L)1}, \phi_{R(L)2}, \phi_{R(L)3}) = \sum_{i=1}^3 E_{Ji} (1 - \cos \phi_{R(L)i}) + E_n^{R(L)}, \quad (7)$$

where $E_{Ji} = E_{JRi} = E_{JLi}$ is the Josephson coupling energy and $E_n^{R(L)} = I_{R(L)}^2/2L_s$ can be represented as

$$E_n^{R(L)} = \frac{\Phi_0^2}{2L_s} \left[n_{R(L)} + f_{R(L)} - \frac{\phi_{R(L)1} + \phi_{R(L)2} + \phi_{R(L)3}}{2\pi} \right]^2. \quad (8)$$

In order to obtain the effective potential of connecting loop, we use the periodic boundary condition over the circumference of connecting loop with self inductance L'_s and obtain the relation for the current in connecting loop such that

$$I' = -\frac{\Phi_0}{L'_s} \left(r - \frac{\phi'_L + \phi'_R + \phi_{R1} - \phi_{L1}}{2\pi} \right), \quad (9)$$

where r is an integer. The superscript prime in this work means the connecting loop. The effective potential of connecting loop with the Josephson coupling energy E'_J can be represented by

$$U'_{\text{eff}}(\phi'_L, \phi'_R, \phi_{R1}, \phi_{L1}) = E'_n + E'_J (1 - \cos \phi'_L) + E'_J (1 - \cos \phi'_R), \quad (10)$$

where

$$E'_n = \frac{\Phi_0^2}{2L'_s} \left[r - \frac{\phi'_L + \phi'_R + \phi_{R1} - \phi_{L1}}{2\pi} \right]^2. \quad (11)$$

The total effective potential, $U_{\text{eff}}^{\text{tot}}$, of the coupled qubit system is given by

$$U_{\text{eff}}^{\text{tot}}(\phi) = U_{\text{eff}}^L(\phi_{L1}, \phi_{L2}, \phi_{L3}) + U_{\text{eff}}^R(\phi_{R1}, \phi_{R2}, \phi_{R3}) + U'_{\text{eff}}(\phi'_L, \phi'_R, \phi_{R1}, \phi_{L1}), \quad (12)$$

where $\phi = (\phi_{L1}, \phi_{L2}, \phi_{L3}, \phi_{R1}, \phi_{R2}, \phi_{R3}, \phi'_L, \phi'_R)$.

The local minima of the total effective potential can be obtained by minimizing the effective potential $U_{\text{eff}}^{\text{tot}}(\phi)$ with respect to ϕ_i , i.e., $\partial U_{\text{eff}}^{\text{tot}}/\partial \phi_i = 0$, which results the current relations at the Josephson junctions as follows:

$$I' + I_R + \frac{2\pi E_{J1}}{\Phi_0} \sin \phi_{R1} = 0, \quad (13)$$

$$-I' + I_L + \frac{2\pi E_{J1}}{\Phi_0} \sin \phi_{L1} = 0, \quad (14)$$

$$I_{R(L)} + \frac{2\pi E_{Ji}}{\Phi_0} \sin \phi_{R(L)i} = 0, \quad (15)$$

$$I' + \frac{2\pi E'_J}{\Phi_0} \sin \phi'_{R(L)} = 0, \quad (16)$$

where $i=2,3$.

The energy of connecting loop depends on current state of each qubit, i.e., diamagnetic or paramagnetic. We express the diamagnetic persistent current state as $|\downarrow\rangle$ and the paramagnetic state as $|\uparrow\rangle$ using spin language. In this scheme one of three junctions in each qubit is included in the connecting loop as can be seen in Fig. 1 (a). The phases of each qubit, ϕ_{L1} and ϕ_{R1} , determine the energy of coupled qubits. Sign of these phases is positive (negative) for diamagnetic (paramagnetic) persistent current. The value of $(\phi_{R1} - \phi_{L1})$ in the periodic boundary condition of Eq. (9) for the connecting loop plays the role of effective external flux in the connecting loop. When one qubit is in the paramagnetic current state and the other in the diamagnetic state, i.e., $|\downarrow\uparrow\rangle$ or $|\uparrow\downarrow\rangle$, the phases ϕ_{R1} and ϕ_{L1} have opposite sign and induce a large value of $(\phi_{R1} - \phi_{L1})$. In this case, the phase difference ϕ'_L and ϕ'_R induced by this effective flux gives the large Josephson coupling energy in the connecting loop. However, when both qubits are in the same current state, i.e., $|\downarrow\downarrow\rangle$ or $|\uparrow\uparrow\rangle$, the phases ϕ_{R1} and ϕ_{L1} have the same sign and are canceled in $(\phi_{R1} - \phi_{L1})$. Then the energy of connecting loop become very small.

The charging energies of Josephson junctions give the kinetic part of Hamiltonian. The number of excess Cooper pair charges on Josephson junction $\hat{N}_i \equiv \hat{Q}_i/q_c$ is conjugate to the phase difference $\hat{\phi}_i$ and the commutation relation $[\hat{\phi}_i, \hat{N}_i] = i$ gives the quantum phase fluctuations of the junction. Using the Josephson relation, $Q_i = C(\Phi_0/2\pi)\dot{\phi}_i$, charging energy, $E_C = \sum_i Q_i^2/2C_i$, becomes

$$E_C = \frac{1}{2} \left(\frac{\Phi_0}{2\pi} \right)^2 \sum_{P=L,R} \left(\sum_{i=1}^3 C_{Pi} \dot{\phi}_{Pi}^2 + C'_P \dot{\phi}_P'^2 \right), \quad (17)$$

where $C_{L(R)i}$ and $C'_{L(R)}$ are the capacitances of the Josephson junctions of the qubit loop and the connecting loop, respectively. If we introduce the canonical momentum $\hat{P}_i \equiv \hat{N}_i \hbar = -i\hbar \partial/\partial \phi_i$ and the effective mass $M_{ij} = (\Phi_0/2\pi)^2 C_i \delta_{ij}$, the Hamiltonian can be given by

$$\hat{H} = \frac{1}{2} \hat{\mathbf{P}}^T \cdot \mathbf{M}^{-1} \cdot \hat{\mathbf{P}} + U_{\text{eff}}^{\text{tot}}(\hat{\phi}), \quad (18)$$

which describes the dynamics of the particle with effective mass M in the effective potential $U_{\text{eff}}^{\text{tot}}(\hat{\phi})$.²

For a given value of the external flux the effective potential of a three-Josephson junction qubit has a double well structure corresponding to the diamagnetic state, $|\downarrow\rangle$, and the paramagnetic state, $|\uparrow\rangle$ at the potential minima. The diamagnetic state and the paramagnetic state have the energy difference depending on the value of the external flux. The charging energy E_C causes quantum tunneling through the barrier of the double well potential resulting the quantum mechanically superposed states. The Hamiltonian describing a qubit then becomes $H_{\text{qubit}} = h_0 \sigma^z + t_0 \sigma^x$, where $2h_0$ is the energy difference between two states, $|\downarrow\rangle$ and $|\uparrow\rangle$, and t_0 is the tunneling amplitude.

For the coupled two qubits, on the other hand, we have four states, $|\downarrow\downarrow\rangle$, $|\downarrow\uparrow\rangle$, $|\uparrow\downarrow\rangle$ and $|\uparrow\uparrow\rangle$, at the effective potential minima for a given value of (f_L, f_R) . Solving coupled equations (13)–(16) in conjunction with Eqs. (6) and (9) numerically, we obtain the local minima of the effective potential of the coupled qubits. We set $\gamma = 200$, $L_s = 11\text{pH}$ and $E_{Ji} = 200\text{GHz}$, which are the design parameters of the qubit of Ref. 3. For the connecting loop we set $\gamma' = \gamma$ and $L'_s = 5L_s$. Obtaining the effective potential minima, $U_{\text{eff}}^{\text{tot}}(\phi_{s,\text{min}})$, we get the energy levels at each potential well,

$$E_s = \frac{1}{2} \hbar \omega_s + U_{\text{eff}}^{\text{tot}}(\phi_{s,\text{min}}), \quad (19)$$

where s denotes the four states, $|\downarrow\downarrow\rangle$, $|\uparrow\uparrow\rangle$, $|\downarrow\uparrow\rangle$ and $|\uparrow\downarrow\rangle$, and $\phi_{s,\text{min}}$ is the value of ϕ_s at the potential minimum corresponding to the state s . The ground state energy, $(1/2)\hbar\omega_s$, can be obtained in harmonic oscillator approximation.² Since the plasma frequency of the

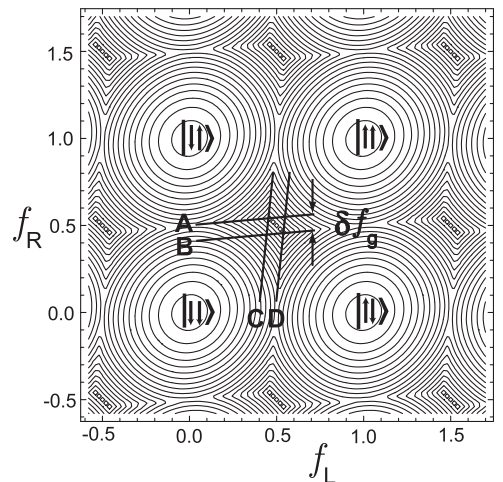


FIG. 2: Ground state energy diagram for coupled current qubits. A,B,C, and D denote the resonance lines and the external flux difference between resonance lines, δf_g , originates from the coupling energy. We consider $E'_J = E_J$.

Josephson junction of the three-Josephson junction loop, $\omega_i = \sqrt{E_{Ji}/(\Phi_0/2\pi)^2 C}$, is larger than the characteristic frequencies, i.e. the level spacing and the amplitude of the tunneling between two states $|\uparrow\rangle$ and $|\downarrow\rangle$, by order of two² and the plasma frequency of the Josephson junctions in the connecting loop can be the same magnitude as that of the qubit loop, we can consider only the ground state energy. By calculating the energy E_s in Eq. (19) for a certain range of (f_L, f_R) , we can obtain four energy planes. In Fig. 2 we show the lowest energy planes and the states of the coupled qubits corresponding to the energy levels. The finite value of δf_g comes from the coupling energy which is higher for different qubit state than the same qubit state. Similar diagrams are shown for coupled charge qubits.^{7,8,14}

The Hamiltonian for the coupled qubits can be written in the two-qubit basis, $|\downarrow\downarrow\rangle, |\uparrow\downarrow\rangle, |\downarrow\uparrow\rangle$, and $|\uparrow\uparrow\rangle$,⁷ from the calculated values of E_s in Eq. (19) as follows,

$$H_{\text{coup}} = \begin{pmatrix} E_{\downarrow\downarrow} & t_L & t_R & 0 \\ t_L & E_{\uparrow\downarrow} & 0 & t_R \\ t_R & 0 & E_{\downarrow\uparrow} & t_L \\ 0 & t_R & t_L & E_{\uparrow\uparrow} \end{pmatrix}, \quad (20)$$

where $t_{L(R)}$ is the tunneling amplitude across the barrier of the double well potential of the left (right) qubit and can be calculated by various methods.^{2,13} These basis states we use do not directly correspond to the individual states without coupling, but to the coupled qubit states characterized by the current states of the two qubits and the connecting loop. A straightforward calculation leads another form of the Hamiltonian H_{coup} ,

$$H_{\text{coup}} = h_L \sigma_L^z \otimes I + h_R I \otimes \sigma_R^z - J \sigma_L^z \otimes \sigma_R^z + t_L \sigma_L^x \otimes I + t_R I \otimes \sigma_R^x \quad (21)$$

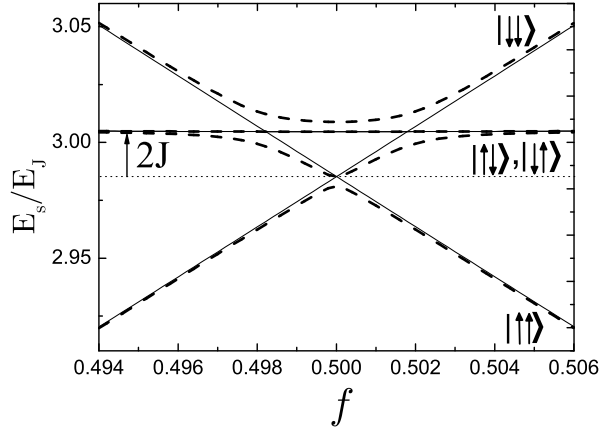


FIG. 3: Energy diagram of the current states of coupled qubits, when $f_L = f_R = f$ and $E'_J = 0.02E_J$. The energies of the coupled qubits without tunneling are represented by solid lines. Dashed lines denote the eigenvalues of H_{coup} in Eq. (20) with $t_L = t_R = 1\text{GHz}$. The energy of antiparallel spin state of coupled qubits shifts upward by amount of $2J$ compared with that of the uncoupled state shown as dotted line.

with relations that $E_{\downarrow\downarrow} = h_L + h_R - J$, $E_{\uparrow\downarrow} = -h_L + h_R + J$, $E_{\downarrow\uparrow} = h_L - h_R + J$ and $E_{\uparrow\uparrow} = -h_L - h_R - J$. Here I is the 2×2 identity matrix and the coupling constant J can be represented as

$$J = \frac{1}{4}(E_{\downarrow\uparrow} + E_{\uparrow\downarrow} - E_{\downarrow\downarrow} - E_{\uparrow\uparrow}), \quad (22)$$

which shows that J is the energy difference between the parallel spin states and the antiparallel spin states as shown in Fig. 3.

Figure 3 shows the energy levels of Fig. 2 along the symmetric line $f_L = f_R$, where the eigenstates of the total Hamiltonian, H_{coup} , are represented as dashed lines. The two-qubit coherent oscillations can be performed at the co-resonance point, $f_L = f_R = 0.5$. The coupled qubits are taken into the co-resonance point from the initial position far away from it and stay for a finite time during which temporal evolution occurs.⁷

III. CONTROLLED-NOT OPERATIONS

We here consider the CNOT operations using evolutions at resonance lines⁸ in Fig. 2 and show that the large value of J in present coupling scheme is able to give accurate CNOT operations. In Fig. 4 the energy levels around lines A and B are shown. Initially the coupled qubits are located far away from the resonance lines, say $f_R = f_L = 0.457$, being represented by the linear combination of the states, $|\downarrow\downarrow\rangle, |\uparrow\downarrow\rangle, |\downarrow\uparrow\rangle$ and $|\uparrow\uparrow\rangle$. When we adjust f_R to the resonance line B in Fig. 4, the evolution from $|\uparrow\downarrow\rangle$ to $|\uparrow\uparrow\rangle$ takes place, and vice versa. However the states, $|\downarrow\downarrow\rangle$ and $|\downarrow\uparrow\rangle$, do not respond to this operation. This discriminating operation enables one to implement the CNOT gate using the left qubit as a control qubit and the right qubit as a target qubit. The

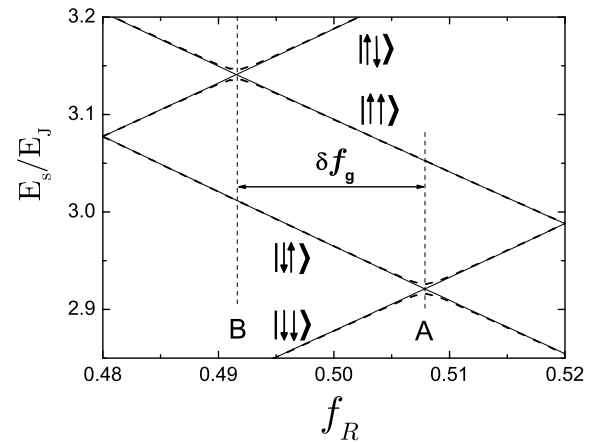


FIG. 4: Energy diagram near the resonance lines A and B when $f_L = 0.48$ and $E'_J = 0.1E_J$. Solid lines represent the energies of the coupled qubits without tunneling and dashed lines are for $t_L = t_R = 1\text{GHz}$. A and B show the values of f_R where the point (f_L, f_R) is on the resonance lines A or B.

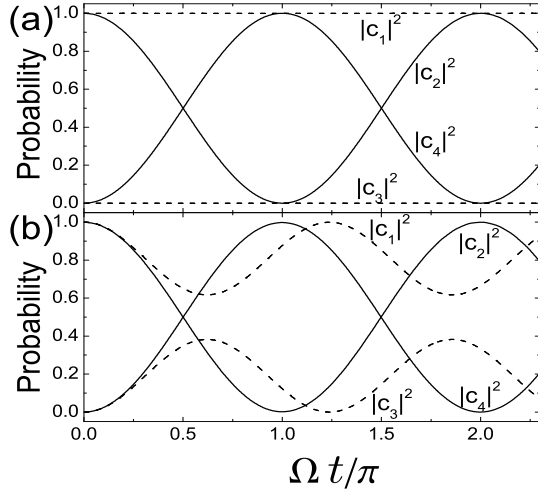


FIG. 5: Time evolutions of the coupled qubits with $t_R = t_L = 0.8\text{GHz}$ for (a) $E'_J = E_J$, $f_R = 0.457$ and $f_L = 0.4837$ and (b) $E'_J = 0.005E_J$, $f_R = 0.4995$ and $f_L = 0.4793$. The solid (dashed) lines display the probabilities that the target (control) qubits occupy the corresponding states.

resonance lines C and D in Fig. 2 are also available, if we want to use the right qubit as a control qubit.

In order to demonstrate the CNOT gate we study the time evolutions of the coupled qubits. We start with the two qubit state written by

$$|\Psi(t)\rangle = c_1|\downarrow\downarrow\rangle + c_2|\uparrow\downarrow\rangle + c_3|\downarrow\uparrow\rangle + c_4|\uparrow\uparrow\rangle. \quad (23)$$

Considering the CNOT gate operation at resonance line B in Fig. 4, we set the initial condition, $c_1 = c_2 = 1$ and $c_3 = c_4 = 0$, at $t = 0$. The time evolution of this state is obtained by the Schrödinger equation, $H\Psi(t) = i\hbar\partial\Psi(t)/\partial t$, with the Hamiltonian in Eq. (20). In Fig. 5 (a) we show the time evolutions of $|c_i|^2$ for the case

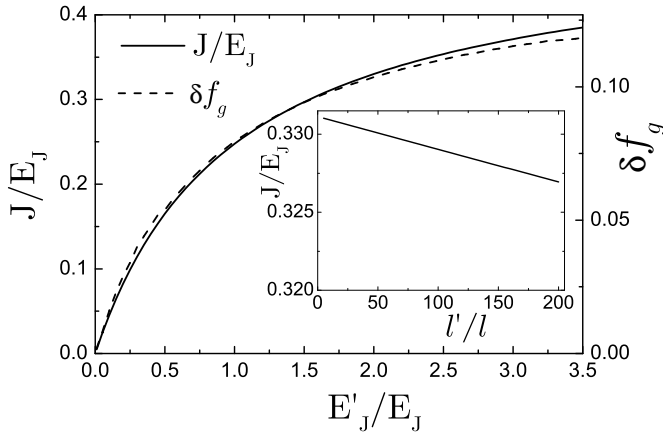


FIG. 6: Plots of the coupling strength J and the external flux difference δf_g versus the Josephson coupling energy in the connecting loop. Inset shows the coupling strength J versus interqubit length l'/l for $E'_J = 2E_J$. Here the coupling strength J is calculated at the co-resonance point $f_L = f_R = 0.5$.

$E'_J = E_J$ and $t_L = t_R = 0.004E_J = 0.8\text{GHz}$. At time $\Omega t \approx \pi$ with $\Omega \equiv 2t_R = 2t_L$ we can see that the state $|\uparrow\downarrow\rangle$ evolves into the state $|\uparrow\uparrow\rangle$, while the states $|\downarrow\downarrow\rangle$ and $|\downarrow\uparrow\rangle$ do not respond this operation. In order to invoke the spin flip between the states $|\downarrow\downarrow\rangle$ and $|\downarrow\uparrow\rangle$ remaining the states $|\uparrow\downarrow\rangle$ and $|\uparrow\uparrow\rangle$ unchanged, the resonance line A can be used for the similar process. Therefore the present scheme completes the CNOT gate operation.

For this discriminating operation the resonance lines A and B should be kept far away from each other. When the target qubit evolves in the CNOT operation, the control qubit must stay in the initial state. However, if the resonance lines are too close, the unwanted oscillation of the control qubit may take place. Thus the design parameters of the coupling scheme should be set for the value of δf_g to be large enough to exhibit high performance of the CNOT gate. In Fig. 4, when f_R is adjusted to line B, the amplitude of the unwanted oscillation between two states, $|\downarrow\downarrow\rangle$ and $|\downarrow\uparrow\rangle$, can be suppressed by the large value of δf_g (or J).⁸ We obtain the values of δf_g and J as a function of E'_J as shown in Fig. 6. We also consider the small δf_g case when $E'_J = 0.005E_J = 1\text{GHz}$ resulting $J = 0.49\text{GHz}$ to investigate how the small coupling strength deteriorates the CNOT gate performance. In Fig. 5 (b) we show the time evolution of the this coupled qubits with the same initial condition as Fig. 5 (a) and $t_L = t_R = 0.8\text{GHz}$, where we can see that the control qubit also evolves and does not stay in the initial state when the target qubit flips at $\Omega t \approx \pi$. Thus we see that the CNOT gate cannot be accomplished in this parameter regime.

Present coupling scheme can achieve large coupling strength by using the phases, not flux, of the phase qubit. With the phase differences, ϕ_{L1} and ϕ_{R1} , of the Josephson junctions in Fig. 1 (a), the effective flux has the value that $f_{\text{eff}} \equiv (\phi_{R1} - \phi_{L1})/2\pi \approx 0.32$ for $f_L \approx 0.5$

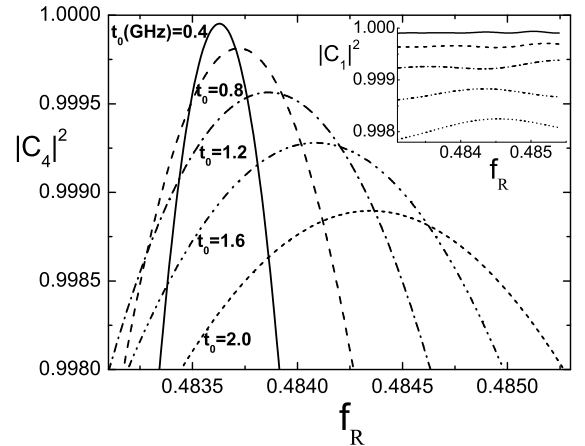


FIG. 7: Switching probabilities of the state $|\uparrow\downarrow\rangle$ to the state $|\uparrow\uparrow\rangle$ of the coupled qubit system when $E'_J = E_J$ and $f_L = 0.457$ for various tunneling amplitudes $t_L = t_R = t_0$. Inset shows the probabilities that the state $|\downarrow\downarrow\rangle$ does not respond to this operation and remains unchanged.

and $f_R \approx 0.5$. The value of coupling strength J can be about $O(E_J)$ with $E_J=200\text{GHz}$ by varying the value of E'_J as shown in Fig. 6, while it is just about 0.5GHz in the experiment using the mutual inductance⁹ since the induced flux of three-Josephson junction loop is quite small¹³ such that $f_{\text{ind}} \equiv \Phi_{\text{ind}}/\Phi_0 \approx 0.002$.

The remaining problem is about the accuracy of CNOT operations. By deliberately choosing the parameter regimes for the implementation of CNOT gate, we can satisfy the fault-tolerant criteria of quantum computation⁵ which is about 10^{-4} . We calculate the switching probabilities for the case in Fig. 5 (a) when $\Omega t \approx \pi$. In Fig. 7 the switching probabilities for various tunneling amplitudes are shown as a function of the external fluxes, f_R , with the fixed value of $f_L = 0.457$ and $E'_J = E_J$. We see in this figure that the fidelity is higher for lower tunneling amplitude. For higher tunneling amplitude, the evolution at a resonance line can be affected by the presence of the other nearby resonance lines. Actually the external fluxes in Fig. 7 correspond to the point in the sector of resonance line B between the lines C and D where the evolution of the left qubit occurs (Fig. 2). The large tunneling amplitude t_L may induce the unwanted oscillation of the control qubit and reduce the fidelity for the state of the target qubit. The slight difference of pick points in Fig. 7 is also attributed to this aspect. We note that, although the probabilities are not so high as in the low t_0 cases, the high t_0 cases have the advantage that the operating ranges of f_R are rather broad than the low t_0 cases. In the inset of Fig. 7 we show the probabilities that the state $|\downarrow\downarrow\rangle$ stays in the initial state.

Many two qubit operations need the controllable coupling strength in implementation. However, the recent experiment on coupled charge qubits^{7,8} and on the coupled current qubits⁹ cannot control the coupling strength. For charge qubits a controllable coupling scheme using variable electric transformer has been proposed theoretically.¹⁴ Present coupling scheme allows

the tunable coupling strength for superconducting current qubit. The Josephson junction in connecting loop is a dc-SQUID which is composed of two Josephson junctions with coupling energy E_{Jx} . Total Josephson coupling energy $E'_J = 2E_{Jx} \cos(\pi f_x)$ is controllable by the finite flux f_x piercing into the dc-SQUID. We show the coupling strength of the coupled qubits J in Eq. (22) as a function of E'_J in Fig. 6.

In addition, we study the dependence of the coupling strength J on the length of the connecting loop, since the length of each connecting loop l' varies with selective coupling in the scalable design of Fig. 1 (b). We plot J as a function of l'/l in the inset of Fig. 6, where J remains almost constant as the value of l'/l increases. This behavior shows that present scheme is appropriate for large scale integration which requires accurate two qubit operations even for very remote qubits.

IV. SUMMARY

We have proposed in this work a scheme of qubit coupling for the persistent current qubits using a connecting loop with Josephson junctions. The Hamiltonian of the coupled qubit system is obtained by calculating the energy levels with the effective potential energy and the kinetic energy originated from the charging energy of the capacitance of the Josephson junctions in qubits and introducing the tunneling through the barrier of the double well potential. The time resolved dynamics shows that the accurate CNOT gate operations can be performed due to the large coupling strength which can be as large as $O(E_J)$. Moreover the coupling strength is controllable and has a weak dependence on the length of connecting loop of two coupled qubits selected from the scalable design.

ACKNOWLEDGMENTS

This work was supported by Korea Research Foundation Grant No. KRF-2003-070-C00020.

* Corresponding author: mdkim@phy.snu.ac.kr

¹ J. E. Mooij, T. P. Orlando, L. Levitov, Lin Tian, Caspar H. van der Wal, and Seth Lloyd, *Science* **285**, 1036 (1999).

² T. P. Orlando, J. E. Mooij, Lin Tian, Caspar H. van der Wal, L. S. Levitov, Seth Lloyd, and J. J. Mazo, *Phys. Rev. B* **60**, 15398 (1999).

³ Caspar H. van der Wal, A. C. J. ter Haar, F. K. Wilhelm, R. N. Schouten, C. J. P. M. Harmans, T. P. Orlando, Seth Lloyd, and J. E. Mooij, *Science* **290**, 773 (2000).

⁴ I. Chiorescu, Y. Nakamura, C. J. P. M. Harmans, and J. E. Mooij, *Science* **299**, 1869 (2003).

⁵ M. A. Nielsen and I. L. Chuang, *Quantum Computation and Quantum Information* (Cambridge University, Cambridge, 2000).

⁶ A. Galindo and M. A. Martín-Delgado, *Rev. Mod. Phys.* **74**, 347 (2002).

⁷ Yu. A. Pashkin, T. Yamamoto, O. Astafiev, Y. Nakamura,

D. V. Averin, and J. S. Tsai, *Nature* **421**, 823 (2003).

⁸ T. Yamamoto, Yu. A. Pashkin, O. Astafiev, Y. Nakamura, and J. S. Tsai, *Nature* **425**, 941 (2003).

⁹ J. B. Majer, F. G. Paaauw, A. C. J. ter Haar, C. J. P. M. Harmans, and J. E. Mooij, cond-mat/0308192 (unpublished).

¹⁰ A. J. Berkley, H. Xu, R. C. Ramos, M. A. Gubrud, F. W. Strauch, P. R. Johnson, J. R. Anderson, A. J. Dragt, C. J. Lobb, and F. C. Wellstood, *Science* **300**, 1548 (2003).

¹¹ M. Tinkham, *Introduction to Superconductivity* (McGraw-Hill, New York, 1996).

¹² K. A. Matveev, A. I. Larkin, and L. I. Glazman, *Phys. Rev. Lett.* **89**, 096802 (2002).

¹³ M. D. Kim, D. Shin, and J. Hong, *Phys. Rev. B* **68**, 134513 (2003).

¹⁴ D. V. Averin and C. Bruder, *Phys. Rev. Lett.* **91**, 057003 (2003).